Coincident Time-of-Flight Measurements of the Velocities of Cf^{252} Fission Fragments*

STANLEY L. WHETSTONE, JR.
Los Alamos Scientific Laboratory, University of California, Los Alamos, New Mexico
(Received 1 February 1963; revised manuscript received 1 April 1963)

The primary object of the experiment was to improve the absolute accuracy of the determination of the mean values of the distributions in fragment velocity, mass, and kinetic energy. Absolute uncertainties attained are estimated to be about $\pm 0.5\%$ for the velocity measurements ($\sim \pm 1\%$ for the energy measurements); statistical uncertainties on the distribution mean values are considerably smaller. Mean velocities of 1.036 and 1.375 cm/nsec, mean mass numbers of 143.61 and 108.39 amu, and mean kinetic energies of 80.01 and 105.71 MeV, respectively, were obtained for the heavy- and light-fragment groups. The mean total-fragment kinetic energy was found to be 185.7 MeV, and the mean mass ratio, 1.334. Perturbations, suggesting fine structure, are found in the primary mass yields. Associated perturbations are observed in the average total-fragment kinetic energy $\langle E_K(R_A)\rangle$ for the corresponding mass divisions. A decrease in $\langle E_K(R_A)\rangle$ near symmetric mass division, extending over five or six mass pairs and reaching about 20 MeV at a mean mass ratio of 1.0, was observed; but the absolute uncertainty is large.

INTRODUCTION

THE nuclide Cf^{252} provides a rare opportunity for the detailed investigation of the spontaneous fission process. Spontaneous fission is of particular interest in the theory of fission because of the simplification introduced by the well-defined initial state of the nucleus undergoing fission. This simplification, however, seems to be compensated for by the fact that the internal energy necessary for spontaneous fission is barely adequate. Also, it has been found that the spontaneous fission of Cf^{252} yields distributions of prompt neutrons and gamma rays, and primary fragment masses and energies, that are complex and difficult to interpret.[1–4]

The great convenience of Cf^{252} as a source of fission fragments and its increasing availability have served to make it an important standard for the calibration of fission-fragment detection systems. This has coincided with the widespread use of semiconductor fragment detectors, which, at the present state of their art, require individual calibration if they are to be used to obtain accurate measurements of fission-fragment energies.[5,6] The absolute calibration of a time-of-flight apparatus is in itself difficult and tedious, so that intercalibrations with Cf^{252} are advisable as well as convenient.

The primary purpose of the present experiment was to improve the absolute accuracy of the simpler distributions in fragment velocity, mass, and kinetic energy. This emphasis, and not the investigation of fine details of the distributions, has dictated the use of longer fragment flight paths at a sacrifice in counting rate, although it is to be expected that the good resolution will make evident sufficiently pronounced fine structure that may occur where there is sufficient yield.

There are obvious needs from the theoretical point of view for more accurate values for the fragment masses and energies. Accurate distributions of primary masses combined with radiochemical mass-yield data make possible good estimates[7] of the neutron emission from individual fragments. Neutron emission probabilities are, of course, closely related to the fragment excitation energies. Kinetic-energy distributions and correlations with mass division are expected to reveal features of the fission process dominated by the Coulomb forces. If it is assumed that the fragment excitation energies reflect the fragment deformations, then the observed neutron emission probabilities, kinetic energies, and mass distributions can be used to infer the possible spatial configurations near the time of the separation of the fragments. This information is important, moreover, in the problem of the detailed "energy balance" of the fission process.[8] It is also important in making systematic comparisons between different fissioning nuclides.[8,9]

The time-of-flight technique of measurement has several important advantages, in contrast to the ionization chamber and semiconductor techniques, for example, that make possible more absolutely accurate determinations of the fragment distributions. From the experimental point of view, the technique requires the well-understood measurements of distance and time, although measurement to the accuracy required of the time intervals between fragment-induced signals in a pair of detectors separated by practical flight distances is still difficult and susceptible to significant error. An additional feature of the time-of-flight technique is the direct way in which the instrumental dispersion (exclu-

* Work performed under the auspices of the U. S. Atomic Energy Commission.

[1] W. E. Stein and S. L. Whetstone, Jr., Phys. Rev. **110**, 476 (1958).
[2] J. C. D. Milton and J. S. Fraser, Phys. Rev. **111**, 877 (1958).
[3] S. L. Whetstone, Jr., Phys. Rev. **114**, 581 (1959).
[4] H. R. Bowman, S. G. Thompson, J. C. D. Milton, and W. J. Swiatecki, Phys. Rev. **126**, 2120 (1962).
[5] H. C. Britt and H. E. Wegner, Rev. Sci. Instr. **34**, 274 (1963).
[6] H. C. Britt, H. E. Wegner, and S. L. Whetstone, Jr., *Nuclear Instruments and Methods* (North-Holland Publishing Company, Amsterdam, 1963).
[7] J. Terrell, Phys. Rev. **127**, 880 (1962).
[8] I. Halpern, Ann. Rev. Nucl. Sci. **9**, 245 (1959); see p. 293.
[9] J. Terrell, Phys. Rev. **113**, 527 (1959).

sive of effects due to inhomogeneities in the source) can be determined. From the theoretical point of view, the double-velocity measurements are influenced much less by the prompt neutron emission than are double-energy measurements. The primary mass and energy distributions are, therefore, obtained more directly; and the ultimate mass resolution, which is limited by the effects of the prompt neutron emission, is, in terms of the standard deviation, better than the ultimate mass resolution of double-energy measurements by a factor of at least 2.[1]

Experimentally, the study of the interesting region near symmetric mass division is made extremely difficult by the great depth and narrow width of the valley of the mass distribution for the spontaneous fission of Cf^{252}. Nevertheless, it was thought that the high resolution of the present measurements justified a more detailed analysis of the behavior of the average total-fragment kinetic energy for these mass divisions.

A much improved source has clearly resulted in data of a quality superior to that of our previous work[1,3]; and better agreement is found with the results obtained at the Chalk River Laboratory,[2] whose results were obtained from a source prepared in a way similar to that used here.

EXPERIMENTAL

The experimental problem is the accurate determination of the initial velocities of both of the fragments in an unbiased sample of the binary fission events. The detection geometry was so arranged that one fragment of each pair detected passed directly from the source to one of two distant detectors. A distribution of initial velocities was thereby obtained, with no corrections for velocity losses required. It is necessary to detect noncollinear events, because of the strong correlations that are known to exist between the effects that produce the deflections of the fragments (the scattering and the recoil from neutron emission) and the important fragment parameters: velocity, mass, and total kinetic energy. Therefore, one of the distant detectors was placed behind a defining aperture that subtended only one-fourth the solid angle subtended by the other. To minimize the rare detection of a coincidence including a fragment scattered from various parts of the apparatus, a loosely collimating system of baffle apertures was used.

Source

The Cf^{252} source was prepared at the Lawrence Radiation Laboratory, Berkeley, by self-transfer from a large electroplated layer to an area of approximately $\pi(3/32)^2$ in.^{2} on nominally 5-μin.-thick nickel foil ($\sim$0.11 mg/cm^2). The initial activity of the deposit was $\sim 3\times 10^4$ fissions/min. The present data were obtained almost two years later. Although no attempts were made to determine accurately the uniformity of the source, visual inspection with a magnifying glass could detect no imperfections. The relatively great thickness of the support foil was to ensure reasonable durability and long life for the precious source. 2-μin. nickel foils have been used for the support of thin sources of more available substances. To minimize the effects due to the thickness of source material and support foil, the plane of the source was oriented at right angles to the direction of the fragment flight paths.

Detectors

A schematic diagram of the detection system, including the pertinent dimensions, is shown in Fig. 1, and represents an improved version of the apparatus and techniques described previously.[1,3]

One fragment from each of the detected pairs of fragments traversed the source backing foil, continued through a 2-μin.-thick nickel foil which was tilted at 45° to the direction of the fragment motion, and then passed down an evacuated flight tube to terminal detector I. Electrons ejected in the forward direction from the tilted nickel foil were accelerated in a direction normal to the plane of the foil and focused to a 0.0005-in.-thick, 1-in.-diam NE 102 plastic fluor, which was glued to the center of the face of an RCA 6810A photomultiplier. This fragment detector, the initial detector, thus supplied the pulse that is used to define the time at which the fragments begin their flights down the measured distances to the terminal detectors.

The other fragment of each detected pair passed directly from the source to terminal detector II, no correction for loss of velocity in foils being necessary. Small losses incurred in the escape from the source material are ignored. A double-baffled oil-diffusion pump maintained a vacuum better than 2×10^{-6} mm Hg in the apparatus.

The terminal detectors were of identical design, each consisting of a thin foil from which electrons are ejected by the impact of the incident fragments, followed by a lens system which accelerates and focuses the electrons to a 0.0005-in.-thick, 1.75-in.-diam NE 102 plastic fluor, heat-formed and glued to the face of an RCA 7264 photomultiplier. The lens design was based on the geometry of the cathode-to-first-dynode section of the RCA 6810 photomultiplier, scaled to larger dimensions. The shape of the curved cathode of the photomultiplier

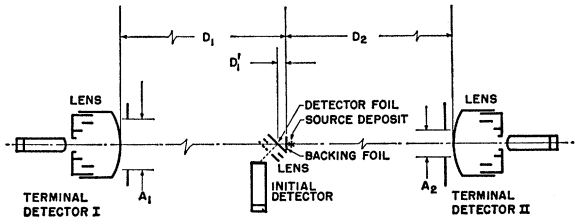

FIG. 1. Schematic diagram of the detection geometry. D_1 = 252.62 cm, D_1' = 3.02 cm, D_2 = 248.07 cm, A_1 = 19.7-cm diam, A_2 = 10.2-cm diam.

was approximated in the fragment detector design by an aluminized VYNS film, about 400 μg/cm^2 thick,[10] stretched smoothly over a ribbed, spherical-cap-shaped structure[11] and then aluminized on both sides. This foil provides a projected area 8 in. in diameter, less approximately 7 in.^{2} of supporting ribs, for the detection of the fission fragments. Tests have shown that for accelerating voltages of approximately 9 kV the differences in the average times for the initiation of the signals from fragments incident on the foil at radii from 0 to 3.5 in. is less than 1 nsec. Pulse-height spectra were measured for each of the detectors to determine conditions that would ensure a nearly 100% detection efficiency for all fragments. Associated measurements of the pulse heights produced by alpha particles from a U^{233} source striking the fluors provided a convenient standard for maintaining the proper over-all gain and discriminator values. Although the terminal detectors had been designed to permit the scintillators to be masked by small circular disks placed on the axis between the source and the detectors, this was found to be unnecessary in the present measurements; the electrons arrive about 10 nsec earlier on the average than those fragments which follow the electrons into the scintillator.[12]

Electronics

The flight times of the fragments were measured using time-to-pulse-height converters.[13] The two converters were started by the pulse obtained from the initial detector. Excessive start rates were avoided by the design of the initial detector, which provided for the shielding of the fluor from alpha particles coming directly from the source. The length of cable between the initial detector and the converter-start input was thus minimized so that the shape of the leading edge of the start pulse was more nearly the same as the shapes of the stop pulses from the terminal detectors. It was necessary, however, to add 65 ft of cable in the output circuit of the initial detector to be able to use the full range of the converters. A single Hewlett-Packard Model 460*B* distributed amplifier preceded by a pulse inverter followed each detector to give the large negative pulses required by the converters. The outputs of the two converters, which are related to the flight times of the two fragments, were processed by 199-channel pulse-height analyzers (gated on by a coincidence between the terminal detectors), and recorded as number pairs on paper tape. The punched tape was subsequently converted to cards, and the analyses performed using a digital computer.

Calibration

The method used to determine the pulse propagation times through the various lengths of cable that were used to calibrate the time-to-pulse-height converters is outlined schematically in Fig. 2. Trace A appearing on the face of the sampling oscilloscope displays pulses produced by a mercury-switch pulser; the second pulse is delayed by a length of cable. The rise time of the first pulse, which has been degraded by the passage through the 120 nsec (~80 ft) scope delay cable, was observed to be about 2 nsec and that of the second pulse, when further degraded by the passage through an additional 130 ft of *RG* 9/*U* cable, was about 3 nsec. (The pulse taken directly out of the pulser can be observed to have a rise time of less than 1 nsec.) Trace B displays the output of the 500 Mc/sec (nominal) shocked oscillator included in the oscilloscope unit. This oscillator can be triggered by the first pulse observed on trace A, so that the two traces maintain a fixed phase relation. The time delay, introduced by the cable, to be measured was determined by sweeping the oscilloscope beams manually along the traces, noting the phase of the 500 Mc/sec wave at the half-height of the leading edges of the two pulses, and counting the cycles in between. The frequency of the shocked oscillator was subsequently determined to be 499.25±0.50 Mc/sec. The time delays produced by a number of lengths of *RG* 9/*U* cable, from 13 to 130 ft, were measured. A good fit to the data was obtained for a delay time directly proportional to the cable length. The velocity of propagation measured in this way was found to be $(1.989\pm0.006)\times10^{10}$ cm/sec or $\beta=v/c=0.6635\pm0.0020$. This indicates an effective dielectric constant $\epsilon=1/\beta^2=2.272\pm0.007$, in agreement

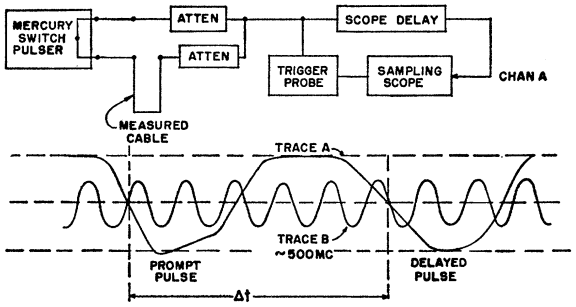

FIG. 2. Schematic diagram of the cable calibration system. Sampling scope: Hewlett-Packard Model 185-*A* (~0.6 nsec rise time); scope delay: ~120 nsec; atten.: 20dB, 51Ω; cable: *RG* 9/*U* (51Ω, coaxial).

[10] Commercially available sturdy Mylar film, 2.5×10^{-4} in. thick (0.9 mg/cm^2), realuminized after mounting, was used in earlier versions of the terminal detectors; this proved to be satisfactory except for a significant reduction of pulse height for the slowest fragments.

[11] The effect of the curved surface of the detector on the uncertainty of fragment flight path can be shown to contribute negligibly to the uncertainty of velocity measurements for any reasonable flight distance.

[12] The so-called "zero-crossing" technique, which was found to improve the timing resolution by 10–20%, was not used in the present measurements because the interference of the pulse from a fragment that follows the electrons into the scintillator with the timing pulse from these electrons was found to delay the triggering of the "stop" discriminators by about 6 nsec.

[13] The Los Alamos Model 23 Converter, an early version of which was described by W. Weber, C. W. Johnstone, and L. Cranberg, Rev. Sci. Instr. **27**, 166 (1956).

with various values quoted for polyethylene.[14] An over-all uncertainty of about $\pm 0.3\%$ is obtained from the following estimates: The uncertainty in locating the half-heights of the two pulses corresponds to about $\pm\frac{1}{8}$ cycles of the 500 Mc/sec wave, or ± 0.25 nsec for each pulse, contributing about ± 0.35 nsec uncertainty to the measured time difference. An additional uncertainty caused by the 1-nsec lengthened rise time of the pulse through the longest (130 ft) cable increases the over-all uncertainty, if the delay for an unattenuated signal is desired, to about ± 0.6 nsec, or about $\pm 0.6/199.2 = \pm 0.3\%$.

The cables so measured were then used to determine the response of the timing system when a prompt pulse was introduced at the output of the initial detector, and pulses delayed by varying known amounts were introduced at the outputs of the terminal detectors. Measurements were made at ~ 10 nsec intervals. The resulting functions $T_1(g_1)$, $T_2(g_2)$ were obtained by interpolation. The responses for zero time differences in the two initial-terminal detector systems were determined by positioning the terminal detectors, one at a time, near to the initial detector and the source. From the results obtained at 9.22 cm, an extrapolation to the condition of zero distance between detectors can safely be made using only approximate values for the velocities involved. In practice, the approximation is iterated if necessary.

In the course of determining the responses for zero time differences, it was found that the responses to heavy fragments (observed in coincidence with fragments in the high-velocity peak in the distant terminal detector) were on the average about 0.5 nsec different from those due to light fragments. A correction for this effect, though small, was incorporated into the calibration tables, assuming a linear dependence with fragment velocity.

The approximately normal distributions of time differences observed with the detectors in the "near" position provide measures of the over-all time resolution of the two detector systems. After subtraction of the effects due to the velocity distributions of the fragments involved, the intrinsic time resolution for the detection of either light or heavy fragments in either detector system was found to have a standard deviation $\sigma = 0.95 \pm 0.15$ nsec or a full width at half-maximum (FWHM) of 2.2 ± 0.4 nsec.

RESULTS

Measurements of the response to nearly zero time differences were made for each detector system before and after the data runs. Changes of only 0.5 and 0.9 nsec were observed. Average values were, therefore, used that were uncertain to about ± 0.5 nsec. During the data runs, pulses derived from a single coaxial mercury-switch pulser were introduced at the outputs of the three detectors so that fiducial responses were obtained at intervals of about 90 min. These served to mark the onset of equipment failure or slow drifts in the calibration. In addition, all gains and thresholds were checked at least once a day. A pulser was used to check the electronics, and alpha sources manipulated from outside the vacuum system were used to check the scintillators and photomultipliers.

In the first run approximately 21 000 events were obtained with an analyzing channel width of about 1.3 nsec, and 8500 more events were obtained at about 1.0 nsec/channel. The terminal detectors were then interchanged and another 12 500 events recorded. Finally, the detectors were restored to their original positions and 2600 more events measured. For the fragments in the "no-foil" channel (II), identical values for the mean velocities of the light- and heavy-fragment peaks were obtained by the two detector systems, within the statistical uncertainty of about $\pm 0.3\%$. Mean velocities of the light fragment peak observed through the foil were also within the statistical uncertainty, but the values for the heavy peak differed by about 0.7%.

Fragment Velocity Distributions

The velocities of the fragments are calculated from the relations

$$V_1 = (D_1 - D_1')/[T_1(g_1) - Z_1],$$

$$V_2 = D_2/[T_2(g_2) + T_1'(V_1) - Z_2],\ T_1'(V_1) = D_1'/V_1,$$

where the subscripts 1 and 2 refer, respectively, to the fragments traversing the two foils and to those traversing no foils. D_1, D_1', and D_2 are distances specified in Fig. 1; Z_1 and Z_2, the "zero-times"[15]; $T_1(g_1)$ and $T_2(g_2)$, the pulse-height-to-time functions; T_1', the time delay of the initial pulse in the V_2 channel.

The observed velocity distributions are shown in Fig. 3(a). The 20 942 events obtained in the first run are used here; the remaining data, spread across a larger range of the pulse-height analyzer, were incomplete, because about 1% of the total events, in the tails of the distribution curves, were not recorded. The distribution $D(V_1)$ has been "smoothed" by transforming pulse-height intervals to velocity intervals by an interpolation procedure, which calculates the fraction of the events recorded in each pulse-height interval that are to be included in a selected velocity interval. This eliminates the fluctuations that arise from recording the data in a finite set of pulse-height intervals rather than directly in velocity intervals. The distribution $D(V_2)$ was automatically smoothed to some degree by the variation of the $T_1'(V_1)$ term in the expression for V_2 for a given

[14] *Reference Data for Radio Engineers*, (International Telephone and Telegraph Corporation, New York, 1956), 4th ed., p. 66; $\epsilon = 2.26$ for stabilized solid polyethylene, *DE*-3401. Also, *Handbook of Chemistry and Physics* (Chemical Rubber Publishing Company, Cleveland, 1962–1963), 44th ed.; $\epsilon = 2.3$.

[15] Z_1 and Z_2 (here, negative numbers) may also be defined as the values of T_1 and $T_2 + T_1'$ corresponding to infinite V_1 and V_2, respectively.

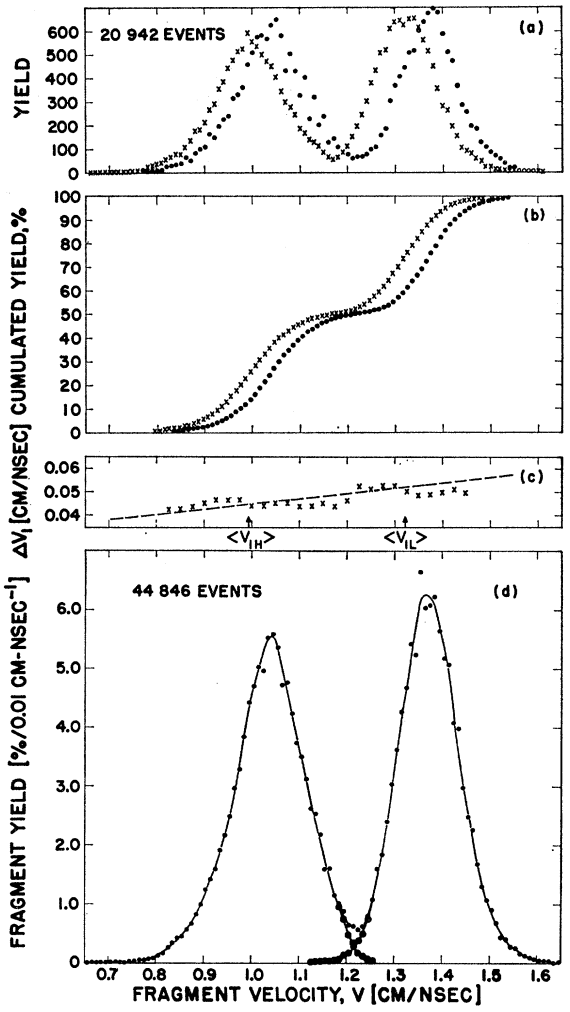

FIG. 3. (a) The observed velocity distributions. ×—$D(V_1)$; ●—$D(V_2)$. (b) The distributions of (a) corrected for "efficiency" and cumulated. (c) The velocity difference $\Delta V_1(V_1)$ caused by the fragments passing through the two foils (see Fig. 1). The straight (dashed) line passes through the points at the average velocities of the heavy and light fragments of the degraded distribution $D(V_1)$. (d) The final velocity distribution $D(V_F)$ from the addition of the distributions $D(V_1)$ and $D(V_2)$, after the correction for the velocity difference $\Delta V_1(V_1)$, but with *no* corrections for "efficiency," normalized to a total yield of 200%. The distributions of the heavy and light fragments are also shown, each normalized to 100%. No corrections have been made for the known small dispersive effects. See Table I for the values of the means and the standard deviations.

channel number g_2; however, it could also have been treated in a similar, though more complicated, way.

As is evident from the relative areas of the peaks in Fig. 3(a), the high- and low-velocity fragments are not recorded with equal efficiencies in the two detectors. The small asymmetry is believed to result from the excessive scattering suffered by the heavier, slower fragments in passing through the foils; the coincidence requirement automatically prevents the complementary lighter, fast fragments from being recorded in the other distribution. Despite the intentionally larger solid angle for the detection of the fragments passing through the foils, there were evidently an appreciable number of scatters to angles greater than 2 to 4 deg.[16] Fragment loss due to small angle scattering was also possibly augmented by areas within the intended detection angle which were rendered insensitive by the foil-supporting ribs required by the terminal detectors.

To obtain the correction required for the velocity lost by the fragments traversing the foils, the two velocity distributions were cumulated[17]; the displacement of the two cumulated distributions parallel to the velocity axis gives the average velocity deficit, $\Delta V_1(V_1)$. Before the distributions are cumulated, however, it is necessary to correct them for the effects attributed to fragment scattering, which may be thought of as a detection inefficiency. The most straightforward way to accomplish this correction is to multiply each of the distributions by a simple function of the velocity to obtain equal numbers of events in the corresponding peaks of the two distributions. The renormalized and cumulated distributions corrected in this way and the velocity losses obtained from them are shown in Figs. 3(b) and 3(c). The step-like velocity dependence of the average velocity loss suggests that the velocity distribution $D(V_1)$ for fragments passing through the foils has been dispersed somewhat more than the distribution $D(V_2)$ for fragments not passing through foils.

The linear approximation $\Delta V_1(V_1)=0.0225+0.0225\ V_1$ (cm/nsec), [obtained by weighting the points according to the degraded distribution $D(V_1)$], shown by the dashed line in Fig. 3(c), was used to shift, event by event, the velocities V_1. The shifted distribution, corrected for efficiency by the appropriate correction function and cumulated, deviates at most by only a few tenths of a percent from the cumulated $D(V_2)$ distribution of Fig. 3(b). Moreover, it can be seen that the complementary nature of the two efficiency corrections brought about by the coincidence requirement ensures that when the properly shifted distributions $D(V_1)$ and $D(V_2)$ are summed, *neither* distribution corrected for efficiency, the resultant distribution, to a good approximation, is free from the distortion attributed to the efficiency effects.

Corrections for the so-called efficiency effects are, therefore, not considered necessary for any of the distributions subsequently discussed; the summing of the distributions obtained in the two directions is expected in each case to remove the largest part of these effects.

The distribution in velocity of all of the data obtained by summing all of the distributions $D(V_1)$ corrected by $\Delta V_1(V_1)$ and the distributions $D(V_2)$, with no corrections made for efficiencies, is shown in Fig. 3(d). The

[16] A dependence of the detection asymmetry on the relative detection solid angles of the two detectors has been observed in other measurements.

[17] This procedure was suggested by the treatment of the mass distributions by Terrell, Ref. 7.

cumulation of this distribution is practically indistinguishable from that shown for $\sum D(V_2)$ in Fig. 3(b). Some of the important parameters of the distribution are given in Table I.

Fortunately, a rigorous treatment of the dispersive effects due to instrumental imperfections and the additional dispersion of the initial velocities due to the prompt neutron emission is not required for the purposes of this paper. The dispersion per fragment of the velocity measurements caused by the instrumental timing uncertainty $\delta T(\approx 2.2\pm 0.4$ nsec FWHM) is given approximately by the formula $(\delta V/V)_I=(V)(\delta T)/D$, where $D(\approx 250$ cm) is the length of the flight path. The relative standard deviation of the initial fragment velocity dispersion caused by recoil when the prompt neutrons are emitted is given by the formula $\sigma_N(V)/V=(\nu_F m_n Q)^{1/2}/P$, where ν_F is the average number of neutrons emitted by the fragments, P is the average momentum of the fragments, m_n is the neutron mass, and $Q=(2/3)\langle E_n\rangle$ is the parameter appearing in the assumed Maxwellian distribution $E_n^{1/2}\exp(-E_n/Q)$ for the center-of-mass neutron energies.[18] The full width at half-maximum value of the dispersion can be expressed by the formula $(\delta V/V)_N=C\nu_F^{1/2}/P$, where $C\approx 2.33$ cm-amu/nsec and $Q=1.0\pm 0.1$ MeV. The results of these estimates are included in Table II. It is evident that the dispersion of the initial velocities in the present measurements is predominantly due to the neutron effects.

On the average, the fragment velocities are altered negligibly by neutron emission when the emission distribution in the fragment frame is symmetric in the forward and backward directions; therefore, the measured velocity distribution is essentially the same as the distribution of initial velocities, if dispersive effects are ignored. The two pronounced peaks in the measured velocity distribution of Fig. 3(d) mirror to some degree the double-peak mass distribution of Fig. 4. The velocity peaks differ in width, with the lower velocity peak about 15% the wider, while the mass peaks, because of mass conservation, are equal in width. The conservation of momentum written as $V=P/A$, would mean that for constant fragment momenta the velocity V and mass A of a fragment would be anticorrelated, and, since $\Delta V=-PA^{-2}\Delta A$, the lower velocity peak (corresponding to the larger masses) would be narrower. (The dispersions due both to the instrumental effects and to the neutron emission also broaden the observed lower velocity peak less than the higher velocity peak.) The average fragment momenta $\langle P\rangle$ are *not* constant, however, but decrease appreciably with increasing mass ratio (probably to a large extent because of the weaker

TABLE I. Mean values and standard deviations of the distributions.[a]

	Direct computation	From Gaussian fits	From data of Milton and Fraser (Ref. 2)
$\langle V_H\rangle$	1.0360 cm/nsec	1.041 cm/nsec	
$\langle V_L\rangle$	1.3750 cm/nsec	1.372 cm/nsec	
$\sigma_0(V_H)$	0.0795 cm/nsec	0.075 cm/nsec	
$\sigma_0(V_L)$	0.0665 cm/nsec	0.063 cm/nsec	
$\sigma(V_H)$	0.0789 cm/nsec		
$\sigma(V_L)$	0.0650 cm/nsec		
$\langle M_H\rangle$	143.61 amu		143.39 amu[b]
$\langle M_L\rangle$	108.39 amu		108.61 amu[b]
$\sigma_0(M_H)$	6.77 amu		
$\sigma_0(M_L)$	6.77 amu		
$\sigma(M_H)$	6.72 amu		
$\sigma(M_L)$	6.72 amu		
$\langle E_H\rangle$	80.01 MeV	80.55±0.11 MeV	79.35±0.13 MeV[c]
$\langle E_L\rangle$	105.71 MeV	106.16±0.06 MeV	103.98±0.08 MeV[c]
$\sigma_0(E_H)$	8.53 MeV	8.62±0.12 MeV	8.40±0.15 MeV[c]
$\sigma_0(E_L)$	5.86 MeV	5.66±0.06 MeV	5.81±0.08 MeV[c]
$\sigma(E_H)$	8.43 MeV		
$\sigma(E_L)$	5.61 MeV		
$\langle E_K\rangle$	185.7 MeV	186.4 MeV	182.7 MeV[d]
$\sigma_0(E_K)$	11.3 MeV	11.3 MeV	11.1 MeV[d]
$\sigma(E_K)$	11.0 MeV		
$\langle R_A\rangle$	1.334		
$\sigma_0(R_A)$	0.150		
$\sigma(R_A)$	0.137		

[a] Absolute uncertainties, roughly 95% confidence limits, are estimated to be about ±0.5% for the mean velocities, about ±1.0% for the mean energies, and less than ±0.5% for the mean mass or mass ratio. Statistical uncertainties are considerably smaller. The standard deviations without subscripts represent the values corrected for the appropriate dispersions given in Table II. The values given under the heading "From Gaussian fits" were obtained by fitting either a single Gaussian curve or a sum of two such curves to the observed distributions, using LASL computer program "PSM," by P. McWilliams, W. S. Hall, and H. E. Wegner, Rev. Sci. Instr. **33**, 70 (1962).

[b] The value given in Ref. 7, p. 885 (106.61) was a typographical error [see Errata, Phys. Rev. **128**, 2925 (1962)].

[c] Data taken from Fig. 11 of Ref. 2 and treated the same way as the data listed under the heading "From Gaussian fits."

[d] Direct computation from data taken from Fig. 9 of Ref. 2. Mean value is the same as that given by authors.

TABLE II. Dispersive effects. (Subscripts I, N, and T refer, respectively, to instrumental, neutron, and combined total dispersive effects.)[a]

	FWHM		Standard deviation
$(\delta V_H/V_H)_I$	0.009	$\sigma_I(V_H)$	0.004 cm/nsec
$(\delta V_L/V_L)_I$	0.012	$\sigma_I(V_L)$	0.007 cm/nsec
$(\delta V_H/V_H)_N$	0.022	$\sigma_N(V_H)$	0.0095 cm/nsec
$(\delta V_L/V_L)_N$	0.022	$\sigma_N(V_L)$	0.0125 cm/nsec
$(\delta_H/V_H)_T$	0.024	$\sigma_T(V_H)$	0.010 cm/nsec
$(\delta V_L/V_L)_T$	0.025	$\sigma_T(V_L)$	0.014 cm/nsec
$(\delta A_F)_N$	1.9 amu	$\sigma_N(A_F)$	0.8 amu
$(\delta A_F)_T$	2.1 amu	$\sigma_T(A_F)$	0.9 amu
$(\delta E_H/E_H)_N$	0.035	$\sigma_N(E_H)$	1.2 MeV
$(\delta E_L/E_L)_N$	0.033	$\sigma_N(E_L)$	1.5 MeV
$(\delta E_H/E_H)_T$	0.038	$\sigma_T(E_H)$	1.3 MeV
$(\delta E_L/E_L)_T$	0.038	$\sigma_T(E_L)$	1.7 MeV
$(\delta E_K/E_K)_N$	0.031	$\sigma_N(E_K)$	2.4 MeV
$(\delta E_K/E_K)_T$	0.034	$\sigma_T(E_K)$	2.7 MeV
$(\delta R_A/R_A)_N$	0.031	$\sigma_N(R_A)$	0.018
$(\delta R_A/R_A)_T$	0.034	$\sigma_T(R_A)$	0.019

[a] Instrumental dispersions are based on the measured standard deviation of the timing uncertainty $\sigma(T)=0.95\pm 0.15$ nsec (2.2 ± 0.3 nsec FWHM) and flight distances of 250 cm. Dispersions caused by neutron emission assume a center-of-mass Maxwellian distribution of neutron energies, $E^{1/2}e^{-E/Q}$, with $Q=1.0\pm 0.1$ MeV, and an average of 1.9 neutrons emitted from each fragment. The values for the full widths at half-maximum (FWHM) are obtained from the relation, valid for normal distributions, FWHM = 2.36 standard deviations. All values given in the table apply for mass ratio $R_A=1.35$. The uncertainty of the instrumental dispersions is about ±15%; the uncertainty of the neutron and total dispersion is less than ±10%. These uncertainties correspond roughly to 95% confidence limits.

[18] It has been shown more generally by Terrell that the magnitude of the dispersive effect, under these assumptions, depends simply on $\langle E_n\rangle$ and not on the *shape* of the emission spectrum. (See Ref. 7.)

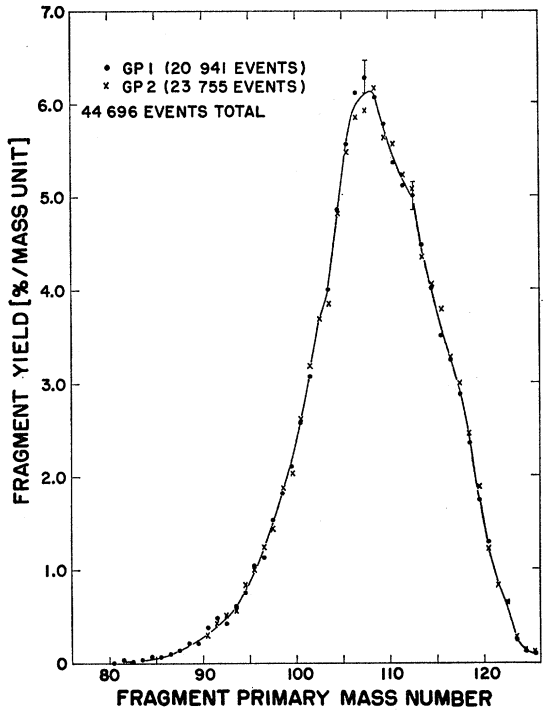

FIG. 4. The observed distribution $D(A_L)$ of the primary fragment masses for the light fragment group, normalized to a total light fragment yield of 100%. ●—1.3 and ×—1.0 nsec analyzer widths. The complete mass distribution curve is necessarily symmetric about the mass number $A_F=M/2=126$. The distributions obtained for two different experimental conditions are plotted separately. The uncertainties assigned to the data points are statistical standard errors. No corrections have been made for the known small dispersive effects. See Table I for the values of the means and the standard deviations.

Coulomb repulsion between the fragments as the charges on the fragments become less equal). The decrease in $\langle P\rangle$ with increasing heavy mass and decreasing light mass, requires that the average velocity of the heavy (slower) fragments change (decrease) at a greater rate than the change (increase) for the lighter (faster) fragments. This is shown in Fig. 7(a). The larger range of average velocities for the slower fragments for all fissions produces the broader peak as observed.

Information concerning possible fine structure in the distributions cannot be expected from these data, because of the limited statistical significance of the data points and the remanent effects of the fluctuations produced by recording the data in pulse-height intervals.

Fragment Mass Distribution

The primary mass[19] of each fragment A_F is determined from the measured velocities, using the conservation laws for mass and linear momentum: $A_L+A_H=M=252$ and $A_H/A_L=V_L/V_H=R_A$. The distribution of the primary light fragment masses is shown in Fig. 4; the complete distribution is necessarily symmetric about the mass number $A_F=126$, one-half the mass number M of the fissioning nucleus. Parameters characterizing the distribution are given in Table I. The dispersion of the measurements of the fragment masses is given in terms of the velocity dispersions δV_L and δV_H, assumed to be independent, found by the formula[3] $\delta A_F=MR_A[(\delta V_L/V_L)^2+(\delta V_H/V_H)^2]^{1/2}/(1+R_A)^2$. The magnitudes of representative dispersive effects are given in Table II.

It is clear, from Fig. 4, that the distribution of the masses in a mass peak is not symmetric about the mean of the peak; the decrease in yield away from the most probable yield is at first more gradual and then more sudden toward the valley than the decrease toward the wings. Moreover, there are four significant deviations from a smooth curve that appear on the steep sides of the distribution near the primary mass pairs 123–129, 118–134, 112–140, and 103–149. The data points obtained with analyzer channel widths of 1.3 and 1.0 nsec have been coded in Fig. 4 to indicate that the deviations are probably not caused by fluctuations attributable to the recording intervals. A fine structure in the primary mass distribution is not unexpected. It is possible that these perturbations, so closely and regularly spaced, are related to the odd-even discontinuities of the mass surface as recently proposed by Vandenbosch and Thomas.[20]

Milton and Fraser,[2] observing a bump near the mass pair 120–132, were willing to attribute this to the effect of a double-magic core of 50 protons and 82 neutrons in the heavy fragment. Some influence of shell structure on the fission process, in particular, for fissions at relatively low excitation energies, can scarcely be denied. It might be expected, however, that shell effects extrapolated from the shell structure of near-spherical nuclei at low excitations are misleading, because of the extreme distortions involved and the proximity of the two fragments, particularly near scission. In any event, all of the perturbations of the primary mass curve observed here are not convincingly explained in terms of the usual magic numbers. Possible fragments from the fission of Cf^{252} containing 50 neutrons or protons or 82 neutrons are included in mass pairs near 124–128, 118–134, and 82–170. The most pronounced perturbation of the mass-yield curve, near the mass pair 112–140, does not correspond very well to the location of any of the magic fragments.

The primary fission-product yield, i.e., the distribution of the fragment masses after the emission of the prompt neutrons, has been determined radiochemically by Nervik.[21,22] Small fine-structure peaks are observed

[19] All of the masses referred to in this paper, A_F, A_H, A_L, and M, are treated as mass numbers. For the conversion to kinetic energies, all of these mass numbers can be equated to atomic mass units to an accuracy of better than 0.1%, in keeping with the neglect of the equally small relativistic corrections.

[20] R. Vandenbosch and T. D. Thomas, Bull. Am. Phys. Soc. **7**, 37 (1962).

[21] W. E. Nervik, Phys. Rev. **119**, 1685 (1960).

[22] Primary fission-product-yield data has also been reported by L. E. Glendenin and E. P. Steinberg, J. Inorg. Nucl. Chem. **1**, 45 (1955) and by J. G. Cunninghame, *ibid.* **6**, 181 (1959).

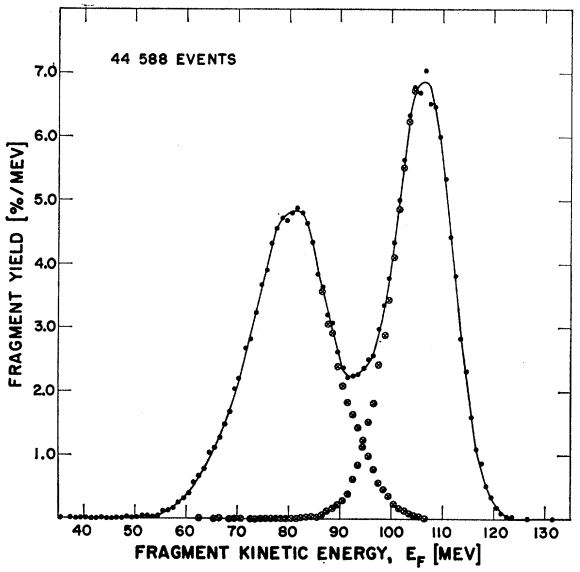

FIG. 5. The observed distribution $D(E_F)$ of the single fragment kinetic energies, normalized to a total yield of 200%. ⊗—heavy- and light-fragment yields, separately, and ●—combined. The distributions of the heavy and light fragments are also shown, each normalized to 100%. No corrections have been made for the known small dispersive effects. See Table I for the values of the means and standard deviations.

at mass 113 and, with greater uncertainty, at mass 135. This agrees with the hypothesis of preferential formation of primary fragments of mass about 135, containing 82 neutrons and emitting almost no prompt neutrons, paired with primary fragments of mass about 117, which emit on the average about 4 prompt neutrons. This neutron emission is in agreement with direct measurements of the average number of prompt neutrons emitted as a function of primary fragment mass.[3,23] It should also be noted that the extremely low primary product yield determined in the radiochemical measurement for mass 125[$(9.3\pm0.4)\times10^{-3}$%] compared to the much larger yield (0.130 ± 0.008%) determined by Nervik[21] for mass 127 may be evidence for the extremely sharp discontinuity predicted[3] in the average number of neutrons emitted at the symmetric primary-mass division at mass 126. This would also imply that the true bottom of the valley for the *primary* mass yield is nearer 0.1%, as measured here, than 0.01%, providing a source of optimism with regard to the effect of the mass resolution on the measured properties near the mass ratio $R_A=1.0$.

Single-Fragment Kinetic-Energy Distributions

The initial kinetic energy of each fragment E_F (the kinetic energy before the emission of prompt neutrons) is determined from its mass and velocity $E_F=CA_FV_F^2$, where $C=0.518$ MeV (amu)$^{-1}$ (nsec)^2 (cm)$^{-2}$. The distribution of the kinetic energies of the individual fragments is shown in Fig. 5, where the distributions of the lower and higher energy members of each pair are shown separately and combined. Parameters characterizing the distributions are given in Table I. The dispersion of the measurements of the single fragment kinetic energies is given in terms of velocity dispersions assumed to be independent, by the formula

$$\delta E_L/E_L=[(\delta V_L/V_L)^2(R_A+2)^2/(R_A+1)^2+(\delta V_H/V_H)^2R_A^2/(R_A+1)^2]^{1/2}.$$

The formula for $\delta E_H/E_H$ is obtained by interchanging the subscripts, including those implied in the mass ratio $R_A=(A_H/A_L)$. The magnitudes of the dispersive effects are given in Table II.

The distributions given in Fig. 5 are useful for the calibration of semiconductor detectors and ionization chambers. For this purpose two characterizations of the peak locations are given in Table I. The difficulty in obtaining a separation of the two peaks is largely overcome with a double-energy detection system that permits the individual energies to be assigned event by event to the higher or lower energy distribution. Since the ionization-type detector observes the final kinetic energies of the fragments, a careful calibration requires that a correction be made for the effects of the prompt neutron emission.[5–7] This requires some knowledge or assumption concerning the average prompt neutron emission from each of the possible fragments.[3,7,23]

Total-Fragment Kinetic-Energy Distribution

The total-fragment kinetic energy E_K, obtained by summing the kinetic energies of the two fragments or from the relation $E_K=0.518M\ V_LV_H$, is distributed as shown in Fig. 6. The distribution reported by Milton and Fraser[2] is also shown. The latter distribution is displaced to energies about 2% lower, and is a few percent narrower at the half-maximum, but somewhat wider at smaller ordinates, than the distribution of the present experiment. The observed shape of this is influenced by the strong correlation [shown in Fig. 8(a)] between the average total-fragment kinetic energy $\langle E_K\rangle$ and the mass ratio R_A. Increased velocity resolution, which tends to narrow the conditional distributions of E_K for a given R_A, is compensated to varying degrees by an increased slope in the $\langle E_K(R_A)\rangle$ dependence, which tends to spread out the over-all marginal distribution of E_K. Parameters characterizing the distribution are given in Table I.

The dispersion of the measurements of E_K are given, for independent velocity dispersions, by the formula $\delta E_K/E_K=[(\delta V_L/V_L)^2+(\delta V_H/V_H)^2]^{\frac{1}{2}}$. The magnitude of the dispersion is given in Table II.

Dependence on Fragment Mass

The regression of the fragment velocity on the mass $\langle V_F(A_F)\rangle$ is shown in Fig. 7(a). This information is necessary to the correction of the data on the numbers

[23] H. R. Bowman, S. G. Thompson, J. C. D. Milton, and W. J. Swiatecki, UCRL-10139, 1962 (unpublished).

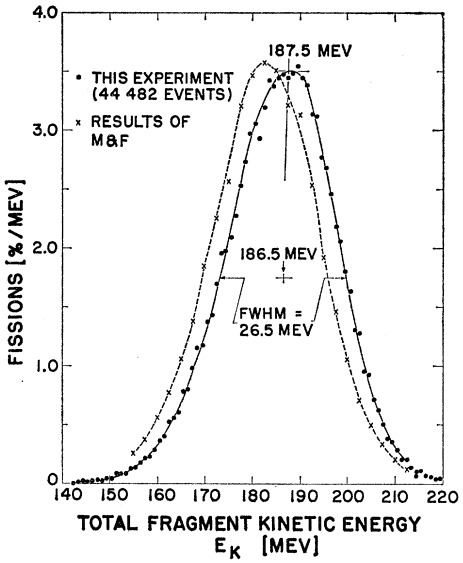

FIG. 6. The observed marginal distribution of the total-fragment kinetic energies $D(E_K)$, normalized to a total of 100%. ●—the results of this experiment, normalized by the number of events in the interval 142–220 MeV; ×—the results of Milton and Fraser, taken from Fig. 9 of Ref. 2, normalized by the number of events in the interval 153.75–213.75 MeV. Shown for the present data are the full-width at half-maximum and the median energies at the maximum and half-maximum, of the distribution. No corrections have been made for the known small dispersive effects. Uncertainties shown are statistical standard errors. Values of the distribution means and standard deviations are given in Table I.

of prompt neutrons (and gamma rays) observed in detectors of solid angles less than 4π sr. It is evident from Fig. 7(a) that a linear dependence of $\langle V_F(A_F)\rangle$, such as that assumed in an early measurement[3] of the average number of neutrons emitted from individual fragments, is an unnecessarily gross approximation.

The regression of the single-fragment kinetic energy on the mass $\langle E_F(A_F)\rangle$ is shown in Fig. 7(b). The most striking feature is the constancy, perhaps accidental, of the average kinetic energy of the lighter fragments. This has also been noted recently for thermal neutron-induced fission.[24]

The regression of the average total-fragment kinetic energy on the mass of the heavy fragment $\langle E_K(M_L)\rangle$ is shown also in Fig. 7(b).

Dependence of Average Total-Fragment Kinetic Energy on Mass Ratio

The regression of the average total-fragment kinetic energy on the fragment mass ratio $\langle E_K(R_A)\rangle$ is shown in Fig. 8(a). Because of the relatively small number of events obtained close to the symmetric mass division, the pronounced dip observed at $R_A=1.0$ in the average total kinetic energy is subject to a large uncertainty. The dispersion of events into the sparsely populated intervals near mass ratio $R_A=1.0$ from the more populated regions at larger values of R_A [see Fig. 8(c)] would be expected to be due chiefly to the dispersion function arising from the recoil from neutron emission, which is usually assumed to be symmetric about the true velocity of a fragment. Since, however, it appears likely that near $R_A=1.0$, almost all of the neutrons are emitted from the light fragment, it is evident that events are dispersed toward symmetry only by decreases in the light fragment velocities, which result in lower measured total fragment energies. Another possible source of spurious symmetric events can arise from unusually large degradations of the fragment velocities in the source or foils. Again it is the faster fragment that must lose velocity, and, consequently, this measured energy is lower. It is interesting, although not conclusive, to note that in Fig. 7(a), *both* the light and heavy fragments show decreases in average velocity near mass number $A_F=126$.

An attempt has been made to remove systematically from the conditional distributions $D_{RA}(E_K)$, shown in Fig. 9, those events, almost certainly spurious, which are dispersed widely from the means of the distributions. The values of $\langle E_K(R_A)\rangle$ that are obtained after this

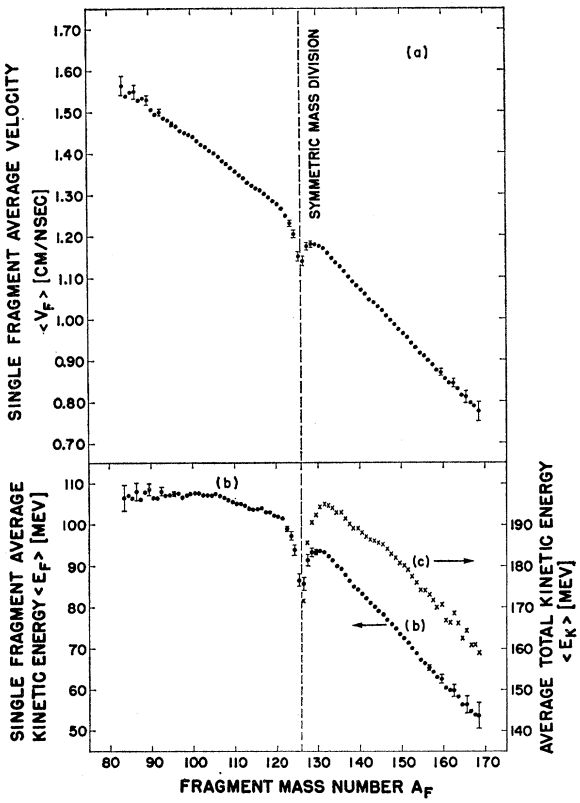

FIG. 7. (a) The regression of the fragment velocities on the fragment mass number. (b) ●—the regression of the single-fragment kinetic energies on the fragment mass number (energy scale to the left); ×—the regression of the total-fragment kinetic energy on the mass of the heavy fragment (energy scale to the right). No corrections have been made for the known dispersive effects. Uncertainties shown are statistical standard errors.

[24] J. C. D. Milton and J. S. Fraser, Can. J. Phys. **40**, 1626 (1962).

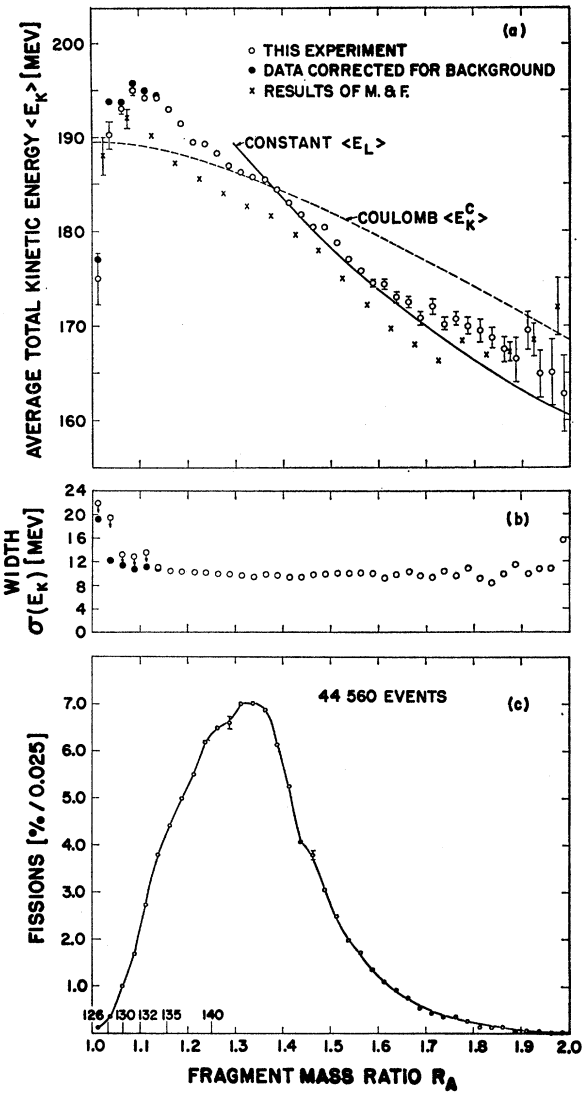

FIG. 8. (a) The regression of the total-fragment kinetic energy E_K on the mass ratio R_A. (The average total-fragment kinetic energy $\langle E_K\rangle$ as a function of the fragment mass ratio $R_A \equiv M_H/M_L$.) ○—the results of this experiment, not corrected; ●—corrected for the small background of lower energy events; (see Fig. 9) ×—the results from Milton and Fraser, Fig. 4 of Ref. 2. The dashed curve shows the dependence of the average total kinetic energy from the simple Coulomb repulsion model (fitted to the data at $R_A=1.3$); the solid curve shows the dependence obtained from the observed constancy of the light-fragment average kinetic energy $E_L(R_A)=107$ MeV. (b) The standard deviations of the conditional distributions of total-fragment kinetic energy for given mass ratio intervals. ○—the results of this experiment, not corrected; ●—corrected for the "background." (c) The marginal distribution of the fragment mass ratios. Corrections for the background are negligible. Values of the distribution mean and standard deviation are given in Table I. No corrections have been made in any case for the known small dispersive effects. Uncertainties shown are relative statistical standard errors.

"background" correction are considered to be more reliable, and they are seen to reduce slightly the magnitude of the kinetic energy dip. An alternative procedure is to estimate an average density of background events from the widely dispersed events occurring in the conditional distribution for a larger interval of mass ratio and then subtract the density of background so obtained from the more limited conditional distributions. The small number of such events in the present data and the possibility of their nonuniform distribution makes the estimate of an average density highly uncertain. This procedure would appear to reduce somewhat more both $\sigma(E_K)$ and the decrease in $\langle E_K\rangle$ for the mass-ratio interval $R_A=1.000$ to 1.025.

The distributions $D_{RA}(E_K)$ shown in Fig. 9, particularly in view of the dependence of the widths of the conditional distributions of total kinetic energy[25] shown in Fig. 8(b), are consistent with the occurrence of a separate mode of symmetric fission, characterized by an average total kinetic energy smaller by 20–30 MeV than that of the asymmetric mode, which is predominant at all mass ratios except those near to $R_A=1.0$. A few more events on the high-energy side of the distribution $D_{RA}(E_K)$ in the interval nearest to $R_A=1.0$ would have helped this interpretation; as it is, the distribution in this interval, although broader, instead of giving the impression of two superimposed high- and low-energy contributions, appears to be shifted as a whole to lower energies.

With respect to the fine structure noted in the mass-yield curve of Fig. 4, it is possible to associate four perturbations evident in the $\langle E_K(R_A)\rangle$ curve, occurring near the mass ratios 1.10, 1.25, 1.35, and 1.45, with four perturbations in the mass-ratio distribution of Fig. 8(c),

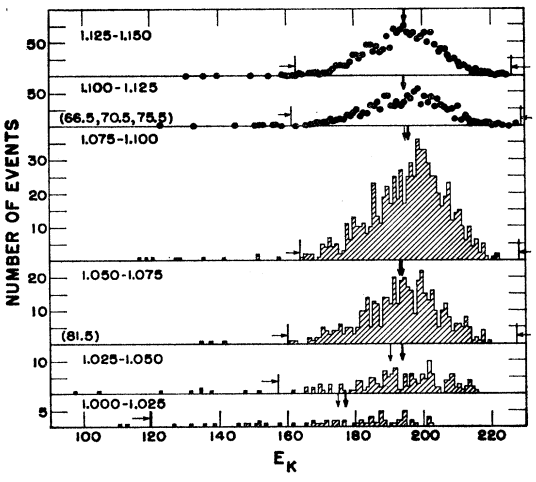

FIG. 9. The observed conditional distributions of the total-fragment kinetic energies for given mass ratio intervals near $R_A=1.0$. The horizontal arrows indicate the limits of the distributions after all events more than three standard deviations distant from the mean are iteratively eliminated. The light vertical arrows indicate the means of the initial distributions; the heavy vertical arrows, the means of the final distributions. Four events (66.5, 70.5, 75.5, 81.5) fall below the lower limit of the graphs.

[25] It is also to be expected that the rapid change of the regression curve $E_K(R_A)$ near $R_A=1.0$ will increase the effect of the dispersions on the widths of the conditional distributions there.

where a deviation is assigned to the large peak at the most probable mass. The chance occurrence of the four correspondences is improbable. The proposal of Vandenbosch and Thomas[20] would seem more likely than an interpretation in terms of shell structure.

The expression

$$E_K = E_L\left(1+\frac{1}{R_A}\right),$$

with E_L=const=107 MeV fits the data of Fig. 8(a) to within $\pm 1\%$ for $R_A=1.3$ to 1.7, and to within $\pm 4\%$ for $R_A=\sim 1.1$ to 2.0. A correction for the dispersive effects increases, in general, the slope of $\langle E_K(R_A)\rangle$, which would improve the agreement with the fitted curve.

Attempts to explain the dependence $\langle E_K(R_A)\rangle$ usually assume that the kinetic energy of the fragments is determined essentially by the potential energy of the repulsive Coulomb interaction at the scission point, when the nuclear attractive interaction between the separating fragments vanishes—neglecting any translational kinetic energy possessed by the fragments at that time. The division of the charge between the two fragments is not known to great accuracy, particularly for the rarer mass divisions. Although the equal-length beta-decay chain hypothesis seems to fit the experiments well, for the purpose of a preliminary investigation of the dependence of the kinetic energy on the mass division, the simpler assumption of unchanged charge ratio, $Z_L/A_L=Z_H/A_H=Z/M=0.3889$, is adequate. With these assumptions, the expressions for the total kinetic energy E_K with the fragments separated to great distances as a function of fragment charge numbers Z_L and Z_H, masses A_L and A_H, and mass ratio $R_A\equiv A_H/A_L$ are

$$E_K{}^c = K_c\frac{Z_LZ_H}{S} = K_c\left(\frac{Z}{M}\right)^2\frac{A_LA_H}{S} = \frac{K_cZ^2}{S}\,\frac{R_A}{(1+R_A)^2},$$

where Z and M are charge and mass number of the initial nucleus, S is the effective distance between the fragment charges at scission (the scission distance), and $K_c=1.440$ MeV-F-(charge number)$^{-2}$.

The dependence $\langle E_K{}^c(R_A)\rangle$ for constant $\langle S\rangle$, where the small error introduced by approximating an average of a product of factors by the product of their averages has been neglected, is shown by the dashed curve in Fig. 8(a), where the average scission distance $\langle S\rangle$ was set equal to 18.24 F to fit the observed data at $R_A=1.30$. It is somewhat surprising to note the large discrepancy between the data and the dependence predicted by the simple Coulomb potential model.

If the mean scission distance $\langle S\rangle$ is allowed to vary with R_A, the data may be fit to the expression for $\langle E_K{}^c(R_A)\rangle$. In Fig. 10 the dependence of $\langle S(R_A)\rangle$, as determined from $\langle E_K(R_A)\rangle$ of Fig. 8(a), is shown by the plotted points. The smooth curve gives the dependence for $\langle E_L\rangle$=const=107 MeV.

The two-sphere model actually suggests a small

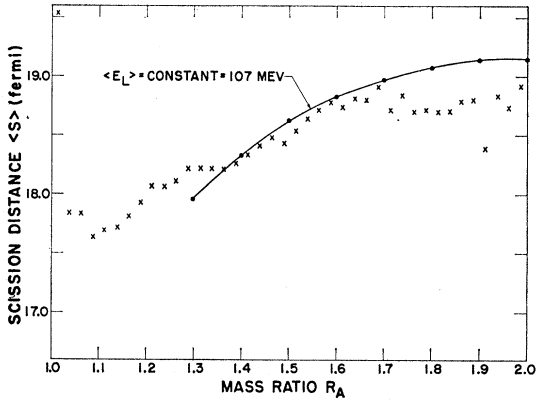

FIG. 10. The mean scission distance $\langle S\rangle$ (the effective distance between the centers of charge of the two fragments at the time of their separation) as a function of the fragment mass ratio R_A calculated from the static Coulomb-potential model, assuming unchanged charge-to-mass ratio. Points are obtained from the fit to the $\langle E_K(R_A)\rangle$ data of Fig. 8(a), the smooth curve from the fit to the data of Fig. 7(b), which gives $\langle E_L(R_A)\rangle=107$ MeV for $R_A=1.3$ to 2.0.

variation of the scission distance as the sum of the fragment radii varies: $\langle S(R_A)\rangle=r_0(A_L{}^{\frac{1}{3}}+A_H{}^{\frac{1}{3}})$. The ratio of kinetic energy releases for symmetric and asymmetric mass divisions is then found to be: $E_K{}^c(1.0)/E_K{}^c(2.0)=(9/8)[S(2.0)/S(1.0)]=1.110$. This is a considerably smaller variation than that observed: $\langle E_K(1.0)\rangle/\langle E_K(2.0)\rangle\approx 195$ MeV/165 MeV=1.18.

The two-sphere model, as has been pointed out by Terrell,[9] also requires a value of r_0 to obtain the proper kinetic energy release that is some 25% greater than the value derived from other experiments. The addition of a third charge-bearing entity in the form of a substantial neck between smaller spheres might be expected to represent the actual situation a little more closely. The neck model[3] can be exhumed temporarily, in its simplest form, where all mass divisions are thought to arise from the same average *spatial* configuration of the nuclear matter at the scission point. A reasonable distribution of the protons and nucleons between the small sphere (S), the large sphere (L), and the neck (N) is the following: $Z_S=33$, $Z_L=49$, $Z_N=16$, $A_S=84$, $A_L=126$, $A_N=42$. Symmetric mass division is assumed to separate the large sphere from the remaining volumes; asymmetric division ($R_A=2.0$), the small sphere. If R_L, R_S, and R_N are the radii of the three volumes, assumed, for the purpose of a simple calculation, to be approximately spherical and with centers on a straight line, the Coulomb potential energies for symmetric and asymmetric mass divisions are given by

$$E_S=K_cZ_LZ_N/(R_L+R_N)+K_cZ_LZ_S/(R_L+R_S+2R_N)$$
$$E_A=K_cZ_SZ_N/(R_S+R_N)+K_cZ_SZ_L/(R_S+R_L+2R_N).$$

For $R_L/R_S=(A_L/A_S)^{1/3}=1.145$, $R_N/R_S\equiv X$, the ratio of the energies is $E_S/E_A=\{0.485[(2.145+2X)/(1+X)]+1\}/\{0.327[(2.145+2X)/(1.145+X)]+1\}$. If the as-

sumption of constant nuclear density is extended to the neck volume, $X \equiv R_N/R_S = (A_N/A_S)^{1/3} = 0.794$. The ratio of the symmetric to very asymmetric kinetic energy release is $E_S/E_A = 1.151$, which is in better agreement with the observed ratio of ~ 1.18. Again assuming a constant nuclear density, the expression for E_S, with $E_S = 195$ MeV, may be solved for the density parameter $r_0 \equiv rA^{-1/3}$. The result, $r_0 = 1.41 \times 10^{-13}$ cm/mass unit, is in good agreement with the values obtained from other experiments.

NOTE

There is recent experimental evidence[26] for a very large increase in the average number of prompt neutrons emitted from nearly symmetric mass divisions for thermal-neutron-induced fission of U^{235}. It would seem that the simple neck model would best survive this phenomenon, as well as the apparently related sudden decrease in the average total-fragment kinetic energy, also near the symmetric mass divisions, if a small fraction of fissions were to occur as a separate mode,[27–31] characterized by a nearly symmetric scission configuration. A test of this symmetric scission configuration would be the determination, either by a direct measurement or by the comparison of primary and secondary mass yield distributions, of the dependence of the prompt neutron emission on fragment mass for the fission of lighter nuclei such as Au, Pb, Bi, and, perhaps, Ra, which are known to favor symmetric mass division.[28,31] The observation of a pronounced saw-toothed dependence of the neutron yield would remove any present justification of the neck model, since the symmetric scission configuration, by the simple mechanism assumed by the model, must give a monotonic dependence.

ACKNOWLEDGMENTS

The preparation of the excellent Cf^{252} source by S. G. Thompson of the Lawrence Radiation Laboratory is gratefully acknowledged. The author is also indebted to J. C. Gursky for the preparation and mounting of the thin plastic films, to W. Shlaer for assistance with the cable measurements, to K. Crandall for much computer coding, and, finally, to J. Terrell for many helpful discussions.

[26] V. F. Apalin, Yu. N. Gritsyuk, I. E. Kutikov, V. I. Lebedev, and L. A. Mikaélyan, Zh. Eksperim. i Teor. Fiz. **43**, 329 (1962) [translation: Soviet Phys—JETP **16**, 235 (1963)].

[27] A. Turkevich and J. B. Niday, Phys. Rev. **84**, 52 (1951).

[28] R. C. Jensen and A. W. Fairhall, Phys. Rev. **109**, 942 (1958); **118**, 771 (1960); A. W. Fairhall, R. C. Jensen, and E. F. Neuzil, in *Proceedings of the Second International Conference on the Peaceful Uses of Atomic Energy, Geneva, 1958* (United Nations, New York, 1958), Vol. 15, p. 452.

[29] J. B. Niday, Phys. Rev. **121**, 1471 (1961).

[30] Yu. A. Selitskiĭ and V. P. Ēismont, Zh. Eksperim. i Teor. Fiz. **43**, 1005 (1962) [translation: Soviet Phys.—JETP **16**, 710 (1963)].

[31] H. C. Britt, H. E. Wegner, and J. Gursky, Phys. Rev. Letters **8**. 98 (1962).